PAPER

Improved electrode kinetics in lithium manganospinel nanoparticles synthesized by hydrothermal methods: identifying and eliminating oxygen vacancies†

Xiaoguang Hao,[a] Olivier Gourdon,[b] Brendan J. Liddle[a] and Bart M. Bartlett*[a]

Lithium-rich manganospinel ($Li_{1+x}Mn_{2-x}O_{4-\delta}$, lithium manganese oxide) has been synthesized by hydrothermal methods employing potassium permanganate, lithium hydroxide, and acetone as synthons. The solid product crystallizes as 30–50 nm particles with some larger 100–300 nm particles also occurring. Materials prepared by this low-temperature route contain oxygen vacancies which can be demonstrated by combining thermogravimetric analysis, differential scanning calorimetry, and cyclic voltammetry. Oxygen vacancies can be minimized beyond the limits of detection for these experiments by annealing the compound in air at 500 °C for 4 h. At room temperature, Rietveld refinement of the powder neutron diffraction pattern shows an orthorhombic $Fddd(\alpha00)$ superlattice of the $Fd\bar{3}m$ space group for hydrothermally synthesized lithium manganospinel. After annealing, oxygen vacancies are eliminated and the superlattice features disappear. Furthermore, the hydrothermal synthesis of lithium manganospinel performed under a pure oxygen atmosphere followed by annealing at 500 °C for 4 h in air gives superior electrochemical properties. This compound shows a reversible capacity of 115 mAh/g when cycled at a rate $C/3$ and retains 93.6% of this capacity after 100 cycles. This same capacity is observed at the faster rate of $3C$. At $5C$, the capacity drops to 99 mAh/g, but capacity retention remains greater than 95% after 100 cycles. Finally, when cycled at $5C$ at an elevated temperature of 55 °C, the O_2 annealed sample shows an initial capacity of 99 mAh/g with 89% capacity retention after 100 cycles. The high rate capability of this material is ascribed to fast lithium-ion diffusion, estimated to be 10^{-7} to 10^{-9} cm^2 s^{-1} by electrochemical impedance spectroscopy.

Introduction

Lithium-ion batteries have emerged as the preeminent technology for electrical energy storage in commercial application such as portable electronics, cellular communication, and even vehicle electrification. A battery is graded on three criteria: energy density, power density, and lifetime; all three need to be as large as possible. In developing chemistry for batteries, new electrode materials or alternative synthesis methods for existing electrode materials are only welcome if they result in improvements based upon these criteria. Accordingly, for any well-established battery material, the race is on to develop synthesis methods that optimize particle size and morphology in such a way that high energy density, high rate capability, and negligible capacity fade distinguish the electrochemistry of the resulting product from similar compositions prepared by tried and true conventional solid-state methods.

In this realm, the spinel structure of lithium manganese oxide, $LiMn_2O_4$, is one of the most well-studied battery materials because, in theory, two lithium ions (and therefore two electrons) can reside in the unit cell giving a range of compositions from $Li_2Mn_2O_4$ to Mn_2O_4 ($=\lambda-MnO_2$).[1,2] As synthesized, $LiMn_2O_4$ is formally mixed-valent Mn^{4+} and Mn^{3+}. However, all manganese ions in the cubic structure are crystallographically equivalent, residing on the 16d Wyckoff site of the $Fd\bar{3}m$ space group.[3] Therefore, it is more appropriate to describe manganese as having an oxidation state of +3.5. In the full range of compositions, this gives an overall gravimetric energy storage capacity of ~285 mAh/g. In practice however, only ~$1/2$ of this capacity is used; as the oxidation state of Mn drops below +3.5, the compound undergoes a symmetry-lowering phase transition

[a] *University of Michigan, Department of Chemistry, 930 N. University Avenue, Ann Arbor, MI, USA. E-mail: bartmb@umich.edu; Fax: +1 734 647 4865; Tel: +1 734 615 9279*

[b] *Jülich Centre for Neutron Science (JCNS) outstation at Spallation Neutron Source (SNS), Oak Ridge National Laboratory, Building 8600, MS-6475 Oak Ridge, TN, USA. E-mail: gourdonoa@ornl.gov; Fax: +1 865 241 5991; Tel: +1 865 576 6629*

† Electronic supplementary information (ESI) available: X-ray diffraction patterns for all samples, N_2 sorption isotherms, FTIR spectra, TGA of the air synthesized sample performed under an N_2 purge, charge-discharge curves for galvanostatic cycling experiments, and Nyquist plots from EIS data. See DOI: 10.1039/c1jm15583k

1578 | *J. Mater. Chem.*, 2012, **22**, 1578–1591

This journal is © The Royal Society of Chemistry 2012

that corresponds directly with the irreversible Jahn–Teller distortion of Mn^{3+}.[4,5] In fact, even if the material is cycled only between the end members Mn_2O_4 and $LiMn_2O_4$ at a potential of ~4.1 V vs. Li^+/Li (where the average oxidation state of manganese remains greater than or equal to +3.5), fracture of micronsized crystallites occurs as the local lithium-ion concentration at the surface increases. The accumulation of Li^+ promotes Mn^{3+} disproportionation into Mn^{4+} and electrolyte-soluble Mn^{2+}.[6] Dissolution of manganese into the electrolyte results in severe and rapid capacity fade. In order to mitigate this surface chemistry and maintain sufficient lithium-ion diffusivity for reasonable kinetics, submicron to micron-sized particles are thought to be ideal.[7]

From a historical perspective, it was almost immediately recognized that the mere presence of the Jahn–Teller active Mn^{3+} ion may render the cubic spinel structure too unstable with respect to other structures and compositions for practical application.[8] However, the many open sites on the spinel lattice (only 1/8 of all tetrahedral sites and only $^1/_2$ of all octahedral sites are filled) and the possibility of non-stoichiometric compositions in the forms of both cation substitution and oxygen vacancies give it a rich chemistry that can be exploited to maintain the cubic structure during electrochemical cycling.[6–12] Moreover, if nanoscale particles can be stabilized such that energy density is not sacrificed due to the aforementioned surface reactions, high power density in lithium manganospinel cells can be realized.[13]

There are many reports on using hydrothermal synthesis to prepare nanoscale lithium manganospinel.[14–28] Most of these methods yield materials with some substitution of lithium for manganese on the 16d sites and also have oxygen vacancies, a well established property of spinels.[29] Substituting lithium on the octahedral sites is beneficial for preventing surface fracture by increasing the manganese oxidation state,[30] but this comes at the expense of some capacity since lithium residing on the 16d sites cannot be extracted. However, oxygen vacancies lower the manganese oxidation state, and the detrimental effects of oxygen vacancies have been well documented in the lithium manganospinel literature.[8,31–35]

Our group recently reported a hydrothermal method for preparing Li-rich spinel nanoparticles by the permanganate oxidation of acetone in an aqueous solution of lithium hydroxide.[36] Here, we report on the presence of oxygen vacancies in our hydrothermally synthesized materials, and we demonstrate that oxygen vacancies can be filled by a subsequent annealing treatment in air. Powder neutron diffraction shows that the synthesized oxygen-deficient compound has an orthorhombic superlattice structure $Fddd(\alpha00)$ where $\alpha = 1/3$ a^*, whereas the annealed compound is cubic ($Fd\bar{3}m$). These small changes in the lattice are imperceptible by Cu-Kα laboratory X-ray diffraction. Electrochemical cells composed of this material show a gravimetric capacity of 115 mAh/g with a cycle-to-cycle capacity retention of >99.9% at a rate of $C/3$ (charge and discharge in three hours). The capacity is unchanged by faster cycling at $3C$ (charge and discharge in 1/3 h), only decreases to ~98 mA h^{-1} at $5C$, and cycles with 88.6% capacity retention after 100 cycles at $5C$ at an elevated temperature of 55 °C. These are excellent characteristics for lithium manganospinel.

Experimental section

1. General considerations

Potassium permanganate 99.0% was purchased from J. T. Baker. Lithium hydroxide 98%, lithium hexfluorphosphate 99.99%, ethylene carbonate and diethyl carbonate solvents were purchased from Aldrich. The solvents were dried over P_2O_5 prior to storing a Vacuum Atmospheres OmniLab glove box under an argon atmosphere. Lithium foil was obtained from Strem Chemicals. Iron(II) chloride (99.5%, argon packed) was purchased from Alfa Aesar. N_2 and O_2 gases (99.99+ %) were purchased from Metro Cyrogenics. HPLC-grade acetone was purchased from EMD Chemicals and distilled prior to use.

Powder X-ray diffraction patterns were obtained with a Brüker D8 Advance diffractometer equipped with a Lynx-Eye detector and parallel beam optics using Cu-Kα radiation ($\lambda = 1.54184$ Å). XRD patterns were indexed and refined using the TOPAS program from Brüker AXS. Scanning electron microscopy images were obtained using a FEI Nova Nanolab SEM/FIB with an accelerating voltage of 10 kV. Infrared spectra were obtained with a Nicolet 6700 FT-IR spectrometer from Thermo Scientific with a MCT-B detector. All the spectra were collected as an average of 5000 scans with 4 cm^{-1} resolution. The BET surface area measurements were obtained from nitrogen sorption isotherms with a NOVA 4200e. All samples were heated in a standard laboratory Fisher vacuum oven 120 °C prior to the measurement. Thermal analysis was obtained with a TGA7 Thermogravimetric Analyzer (Perkin Elmer) at a heating rate of 10 °C under air or nitrogen flow, and differential scanning calorimetry was obtained with a DSC Q10 (TA instruments) at a heating rate of 10 °C. DSC data were analyzed by the Universal Analysis 2000 software package.

2. Hydrothermal synthesis and annealing

All of the spinel-structured compounds in this study were prepared by hydrothermal treatment of 0.158 g (1.00 mmol) $KMnO_4$ in 12 mL 0.1 M LiOH(aq) with 1.00 mmol of acetone in a similar manner to what have previously described.[36] Reactions were carried out in 23 mL PTFE-lined, stainless-steel Parr autoclaves which were sealed in a Plas-Lab wet box. Here, the lithium hydroxide solution was purged with N_2 gas or O_2 gas prior to sealing in the wet box under the same N_2 or O_2 atmosphere where appropriate. Autoclaves were heated to 200 °C at a rate of 10 °C min^{-1}. After a dwell time of five hours, reactions were cooled to room temperature at a rate of 5 °C min^{-1}. Dark green microcrystalline powders were collected by centrifugation, washed several times with deionized water, and dried overnight in a vacuum oven at 120 °C. Subsequent annealing was performed in an MTI compact muffle furnace at 500 °C for 4h under ambient room atmosphere.

3. Elemental analysis

ICP-AES elemental analysis for Li and Mn was obtained using a Perkin-Elmer Optima 2000DV. Samples were digested in 3–5 mL conc. HNO_3 with a few drops of H_2O_2. Samples were references to an yttrium internal standard and concentrations of lithium and manganese were determined from the maximum

intensity lines (610.632 nm for Li; 257.610 nm for Mn) compared to those of standard reference solutions. The average oxidation states of manganese were determined by a potentiometric titration using $FeCl_2/KMnO_4$. 20 mg samples were digested in 0.020 M $FeCl_2$ solutions of 10% H_2SO_4 that were titrated against 4.68 mM $KMnO_4$ according to the balanced equation:

$$5Fe^{2+}(aq) + MnO_4^-(aq) + 8H^+(aq) \rightarrow 5Fe^{3+}(aq) + Mn^{2+}(aq) + 4H_2O(l)$$

4. Electrochemical measurements

Active cathode mixtures were prepared by mixing the synthesized spinel material, carbon black and poly(vinylidene) fluoride (PVDF) using a mass ratio of 75 : 15 : 10 with a Thinky AR-100 rotation/revolution super mixer. *N*-methyl-2-pyrrolidone (NMP) was added to dissolve the PVDF and to maintain appropriate viscosity of the black slurry. This material was coated onto a de-oiled aluminum foil using the doctor blade method. Then, the foil was dried in the vacuum oven overnight at 120 °C prior to assembling the cell in order to minimize surface-bound water as best as possible.[37] The cathode and Celgard™ poly(propylene) film were cut and fit into a $^1/_4$ ″ Swagelok™ PTFE union under ambient room atmosphere. The partially assembled cell was then pumped into a Vacuum Atmospheres OmniLab glove box under argon, where cell assembly was completed. The electrolyte solution was composed of 1 M $LiPF_6$ in 2 : 1 (v/v) ethylene carbonate and diethyl carbonate, and lithium foil was used as the anode.

Cyclic voltammetry measurements were performed on an eight-channel CH Instruments 1000 Electrochemical Workstation at a scan rate of 0.1 mV s^{-1}. Gavlanostatic charge/discharge measurements at the rate C/10 were recorded with CH Instruments 660C Electrochemical Workstation. Higher current charge/discharge curves were recorded on a custom-designed Vencon UBA5 battery analyzer. Cycling at 55 °C was accomplished by submerging the Swagelok cell into a heated sand bath maintained at constant temperature using a Variac transformer.

Electrochemical impedance spectra (EIS) were recorded on an Autolab PGSTAT302N with a FRA (frequency response analysis) module. Prior to EIS measurements, the cells were cycled 3 times between 3.4 and 4.45 V at current C/3. Then the EIS were recorded at various requested potentials from 4.00 to 4.40 V with a 1 h equilibrium time such that the current flow declined to less than 5 nA. The AC perturbation was ±10 mV, and the frequency range was from 10^5 to 10^{-2} Hz. Data were fit using the Zview™ software package.

5. Powder neutron diffraction

Time-of-flight neutron diffraction experiments for air synthesized and air annealed samples were performed on a powder diffractometer (POWGEN) in a vanadium can sample holder by applying a spallation neutron source (SNS) at ORNL (Oak Ridge National Lab). Differing from nearly all other time-of-flight (TOF) neutron powder diffractometers, the design of POWGEN is based on combining the diffracted neutrons collected at all angles into a single profile rather than assigning them to series of different profiles that traditionally were based on grouping detectors according to scattering angle. Such

a unique approach yields to a high count rate while preserving good resolution $\Delta d/d = 0.0015$ at $d = 1$ Å. The diffraction data were collected at 293 K using incident neutron beam wavelengths centered at 1.066 Å and 3.198 Å for d-spacing ranges of 0.29–3.09 Å and 1.47–7.21 Å, respectively. The collected diffraction patterns were calibrated using a LaB_6 standard before Rietveld refinement using the software Jana2006.

Results

1. Establishing composition by ICP-AES, and potentiometric titration

The lithium manganese oxide spinel compounds in this study were prepared by hydrothermal synthesis starting from potassium permanganate, lithium hydroxide, and acetone according to the balanced equation:

$$4LiOH(aq) + 8KMnO_4(aq) + 6(CH_3)_2CO(l) \rightarrow 4LiMn_2O_4(s) + 6CH_3COCHO(l) + 8KOH(aq) + 4H_2O(l) + O_2(g) \quad (1)$$
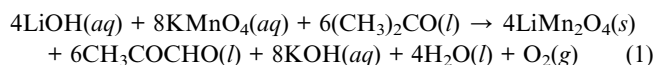
In order to form spinel as the only solid-state product of the reaction (*i.e.*—without the common Mn_3O_4 haussmanite impurity present), we have discovered that reactions performed in a total volume of 12 mL of 0.1 M LiOH (1.20 mmol) with 1.00 mmol $KMnO_4$ and 1.00 mmol $(CH_3)_2CO$ heated to 200 °C for 5 h are ideal. We have previously shown that pyruvaldehyde can be isolated from reaction mixture once the vessels have cooled.[36] Moreover, when considering the excess base added to the reaction, the ratio of LiOH to $KMnO_4$ remains 1 : 2 in the balanced equation even for the complete 16-electron oxidation of acetone to carbon dioxide:

$$16LiOH(aq) + 32KMnO_4(aq) + 7(CH_3)_2CO(l) \rightarrow 16LiMn_2O_4(s) + 21CO_2(g) + 32KOH(aq) + 13H_2O(l) \quad (2)$$
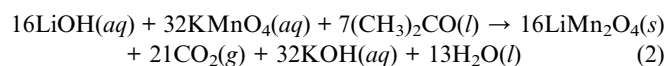
The solid product in the balanced equations above is written as stoichiometric $LiMn_2O_4$. Fig. 1 shows the X-ray diffraction pattern of lithium manganospinel synthesized using the hydrothermal conditions described above, noting that the vessels are sealed under the ambient room atmosphere. The lattice parameter is slightly smaller for this compound compared to that of stoichiometric $LiMn_2O_4$, (8.242 *cf.* 8.248 Å). The compound $LiMn_2O_4$ is formally mixed-valent with an average manganese valence, Z_{Mn}, of exactly 3.5. However, in the structure, manganese resides on a special position (16d octahedral sites) such that all manganese ions are symmetrically equivalent, related by a three-fold inversion axis and a mirror plane. A smaller lattice constant implies that the average manganese valence is greater than 3.5, and one way to accomplish this is the aliovalent substitution of lithium for manganese on the octahedral sites, where the average oxidation state of manganese must increase to maintain electroneutrality:

$$Li_{1+x}Mn_{2-x}O_4 \equiv [Li]_{8a}[Li_x,Mn_{2-x}]_{16d}[O_4]_{32e} \quad (3)$$
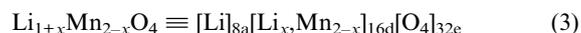
where the subscripts outside brackets denote Wyckoff positions on the spinel lattice. Mn^{4+} is smaller (6-coordinate, high spin ionic radius = 0.67 Å) than is Mn^{3+} (0.72 Å), and the average oxidation state of manganese, Z_{Mn}, is related to the degree of ion

1580 | *J. Mater. Chem.*, 2012, **22**, 1578–1591

This journal is © The Royal Society of Chemistry 2012
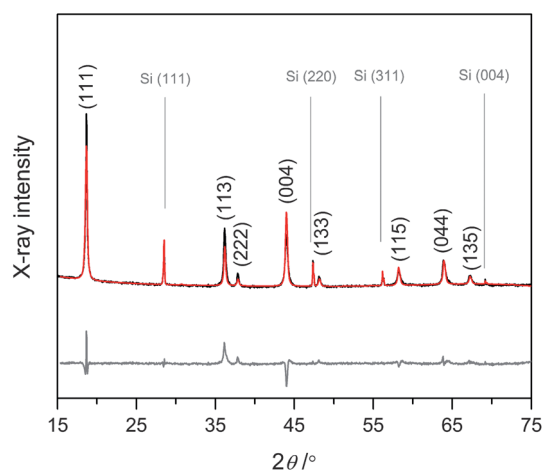
Fig. 1 X-ray diffraction pattern of lithium manganospinel synthesized in air under hydrothermal conditions. The black, red, and gray traces represent the experimental pattern, the Rietveld refinement, and the difference pattern respectively. Miller indices for lithium manganospinel are shown in black. 10% silicon was added as an internal reference and its Miller indices are shown in gray.

substitution by $\frac{7-x}{2-x}$. The compound is still considered to be stoichiometric because the total number of cations in the formula unit remains 3 and the number of anions is 4.

ICP-AES analysis confirms that compounds prepared by our hydrothermal synthesis have a Li:Mn ratio greater than 0.5. However, potentiometric titration of manganese against ferrous iron gives a surprisingly smaller Z_{Mn} of +3.47. This, hints that cation substitution alone does not tell the full story of spinel synthesized by hydrothermal methods. Rather, vacancies in the oxygen sublattice, a nonstoichiometric defect in the spinel structure, must also be considered. To demonstrate further the presence of oxygen vacancies that result from hydrothermal synthesis, we observe that the lattice parameter gets smaller still (8.228 Å) and Z_{Mn} increases (+3.57) after annealing the sample in air at 500 °C for 4 h. Importantly, ICP-AES shows that the Li: Mn ratio is unchanged after annealing. We can understand our diffraction and titration results by considering first the formula for spinel with no cation substitution but with oxygen vacancies, $LiMn_2O_{4-\delta}$. Here, Z_{Mn} is given by $\frac{7-2\delta}{2}$, where the presence of oxygen vacancies lowers Z_{Mn}. By annealing in air, atmospheric oxygen is reduced at the surface and fills in these vacancies according to the reactions:

$$\delta/2\ O_2(g) \rightarrow \delta(O_{ads}) \qquad (4)$$

$$\delta(\square_O^{\cdot\cdot}) + \delta(O_{ads}) + 2\delta e' \rightarrow \delta(O_O^\times) \qquad (5)$$
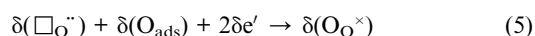
in the standard Kröger-Vink notation. Notably, the electrons in eqn (5) are transferred from manganese; thus filling in oxygen vacancies increases Z_{Mn}.

Therefore, in compounds prepared by hydrothermal methods, the overall formula is best represented as having both cation substitution and oxygen vacancies, $Li_{1+x}Mn_{2-x}O_{4-\delta}$. Now, Z_{Mn} is determined by the formula $\frac{7-x-2\delta}{2-x}$. The mole fraction of lithium that substitutes on the 16d sites, x, can be measured

directly from the Li:Mn ratio from ICP-AES analysis. We cannot analyze directly for oxygen using this technique, but we can couple x with Z_{Mn} from our titration data to estimate δ, the oxygen non-stoichiometry. Table 1 compares elemental analysis data and X-ray data for all synthesized and annealed samples. The monikers "air," "N₂" and "O₂" in the text, table, and figure captions refer only to the atmosphere under which the hydrothermal reaction was carried out. Then, the terms "synthesized" and "annealed" refer to those compounds studied directly upon filtering the products under ambient conditions and those compounds that were subsequently annealed in air at 500 °C for 4 h, respectively.

2. Altering the oxygen stoichiometry through synthesis

Hydrothermal synthesis is performed under constant volume, and we have prepared spinel-structured compounds in vessels sealed under ambient room atmosphere, under a pure nitrogen atmosphere, and under a pure oxygen atmosphere (99.99% gas purity) in order to compare the degree of cation substitution and oxygen vacancies that result. To ensure a pure atmosphere, the aqueous lithium hydroxide solution was thoroughly purged (at least 2 h) with the gas of interest prior to starting the reaction. Table 1 shows that as we increase the partial pressure of oxygen in the reaction vessel, we observe fewer oxygen vacancies in the synthesized spinel product (determined from ICP and titration data). Rietveld refinement of XRD data shows that as the oxygen content of the synthesis atmosphere increases from 0% (N₂) to 100% (O₂), the lattice parameter, a, indeed decreases from 8.244 Å to 8.223 Å when assigned to the space group $Fd\bar{3}m$. After annealing these samples at 500 °C for 4 h in air, we observe the same trend: a decreases and Z_{Mn} increases. X-ray diffraction patterns with for all compounds is presented in Fig S1.† In a control experiment, we find that heat alone does not result in a smaller unit cell or increased Z_{Mn}; in fact, annealing lithium manganospinels in pure N₂ at 500 °C results in a slight increase of a to 8.250 Å (Fig S2†), and Z_{Mn} is +3.31.

All of the spinel compounds prepared in this study crystallize as nanoparticles with a mean size of ~30 nm, illustrated in the SEM image of Fig. 2. Interspersed in these nanoparticles are some larger 100–300 nm particles. Important to our work, particle size is conserved upon annealing—that is, no interfacial crystal growth occurs at 500 °C. In addition, nitrogen sorption isotherms in Fig S3† show that hydrothermally synthesized lithium manganospinels have surface areas (determined by the BET method) on the order of 60 m² g⁻¹, but show type-II (non-porous) behavior. These areas are similar to those observed in materials prepared by calcination of lithium salts and electrolytic grade manganese oxide at temperatures below 500 °C.[9]

3. Observing lattice distortion by PND

The X-ray scattering factor for lithium is small as it scales with atomic number ($Z = 3$). Therefore, we turned to powder neutron diffraction to determine the structure and site occupancy factors for lithium manganospinel. $LiMn_2O_4$ known from the literature adopts the cubic $Fd\bar{3}m$ structure, therefore, as a first attempt such cubic symmetry was used to refined the data collected on the $LiMn_2O_4$ synthesized in the air. However, such refinement leads

Table 1 Characterization and electrochemistry of lithium manganospinels compared in this study

	Air synthesized	Air annealed	N_2 synthesized	N_2 annealed	O_2 synthesized	O_2 annealed
$a/\text{Å}$	8.242	8.228	8.244	8.230	8.230	8.221
Li:Mn	0.508	0.508	0.504	0.504	0.506	0.506
Z_{Mn}	3.47	3.57	3.45	3.55	3.47	3.58
Empirical formula	$Li_{1.01}Mn_{1.99}O_{3.95}$	$Li_{1.01}Mn_{1.99}O_{4.06}$	$Li_{1.01}Mn_{1.99}O_{3.94}$	$Li_{1.01}Mn_{1.99}O_{4.04}$	$Li_{1.01}Mn_{1.99}O_{3.96}$	$Li_{1.01}Mn_{1.99}O_{4.07}$
SA ($m^2\ g^{-1}$)	65.5	54.6	61.7	68.1	56.0	59.5
Initial capacity at C/10 (mAh/g)	138	137	127	132	144	118
Initial discharge at C/10 (mAh/g)	117	106	116	124	116	112
Discharge capacity at C/3 (mAh/g)	114–86	122–101	116–87	116–91	120–108	115–108
% Capacity fade after 100 cycles at C/3	25.0	17.2	25.0	21.6	10.0	6.1

to a poor reliability factor and the difference curves on the refinement showed poor agreement, particularly with the (004) reflection. As shown in the inset of the Fig. 3a, this $(004)_c$ reflection, could be better described by the three independent reflections {(004), (040) and (400)}. Therefore, refinement using a $Fddd$ orthorhombic symmetry (a subgroup of $Fd\bar{3}m$) was performed, leading to a noticeable improvement of the refinement to a satisfactory $R = 7.3\%$. The pattern is shown in Fig. 3, and the cell parameters refined as $a = 8.2808(3)$ Å, $b = 8.2133(3)$ Å and $c = 8.24006(3)$ Å.

At this stage of refinement, we note an unusually large atomic displacement parameter (ADP) on the oxygen site. Since such behavior is characteristic of non-stoichiometry in oxides, the oxygen occupancy was refined and converged to 96(1)% with a significant improvement of the refinement ($R = 6.7\%$ for

a $G.o.F. = 2.3$). Table 2 lists the atomic positions, ADP and occupation parameters for $LiMn_2O_{3.96}$ synthesized in the air. PND cannot differentiate 1% substitution of Li for Mn on the 16d sites (surmised from our ICP results), but we note that the unit cell parameters support this formulation. For the last step of the refinement, some weak reflections that are still not indexed remain noticeable. These reflections could be indexed as first-order satellites of a commensurate tripling along the a direction of the average unit cell. As the number of parameters to refine will drastically increase, a superspace approach of the commensurate modulation has been preferred to a supercell one. Therefore the superspace group $Fddd(\alpha00)$ with $\alpha = 1/3\ a^*$ was used to refine the structure fully. (For a comprehensive description of $(3+n)$-dimensional crystallography, see, for instance, works by Janssen *et al.*[38] and van Smaalen[39] and references within.) The
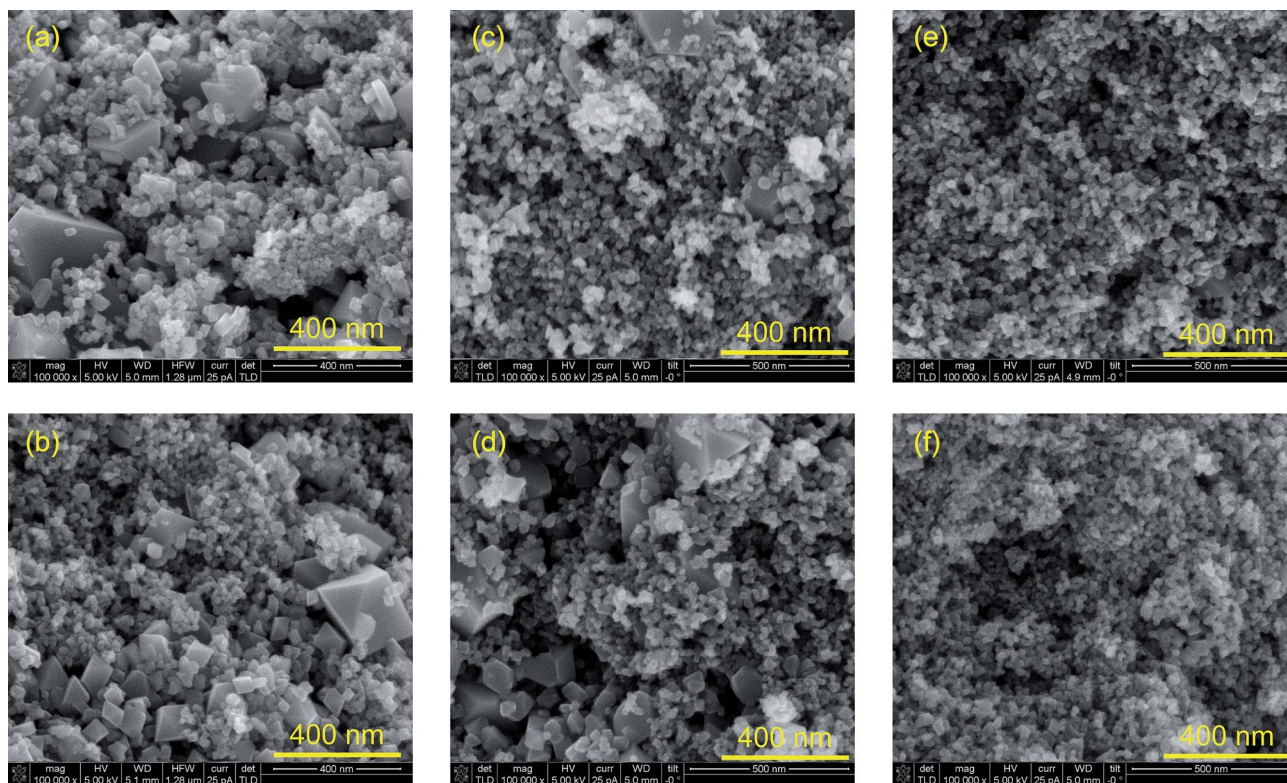
Fig. 2 SEM images of lithium manganospinels synthesized by hydrothermal methods: a) air synthesized; b) air annealed; c) N_2 synthesized; d) N_2 annealed; e) O_2 synthesized; f) O_2 annealed.
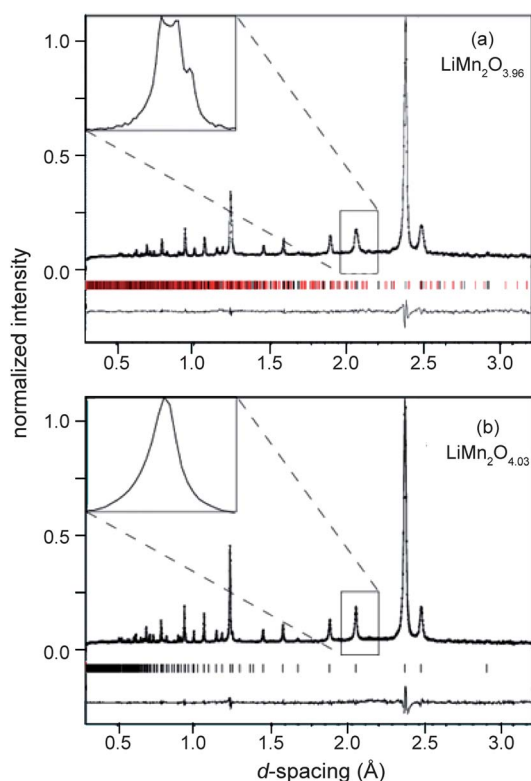
Fig. 3 Neutron powder pattern obtained on POWGEN at 300 K on (a) $LiMn_2O_{3.96}$ synthesized in air and (b) the annealed $LiMn_2O_{4.03}$ sample. Dots indicate the normalized profile, the solid line is the calculated profile, tick marks below profile indicate the positions of all allowed reflections, and the difference curve is show below the tick marks on the same scale (d-spacing range 0.30–3.2 Å). In the case of $LiMn_2O_{3.96}$, black and red tick marks indicate main and satellite reflections, respectively (see text for details). The insets present an expanded region around the $(004)_c$ reflection.

Fig. 4 Representation of the atomic modulations on (a) the oxygen occupancy and (b) the manganese displacement along the a direction. The dashed lines represent the commensurate sections.

superspace model of this crystal structure has been obtained by subsequent introduction of modulation parameters on atomic positions and site occupancies. Such an approach has led to introducing one modulation wave on the Mn atomic position and one modulation wave on the oxygen occupancy. These modulations are presented in Fig. 4 and red tick marks on the Fig. 3a illustrate the position of these satellite reflections. The modulations parameters are classically written as:

$$u\left(\overline{x}_4^{\nu}\right) = \sum_{n=1}^{k} s_n \sin\left(2\pi n \overline{x}_4^{\nu}\right) + \sum_{n=1}^{k} c_n \cos\left(2\pi n \overline{x}_4^{\nu}\right) \qquad (6)$$

with s_n and c_n being the *refined* coefficients of the nth order harmonic. Using this formalism, the modulation wave on the oxygen occupancy imply $s_1 = 0.16(4)$ and $c_1 = 0.13(3)$. For the

Mn atomic displacement only sine terms have been used with $s_1 = -0.0118(15)$, $0.002(4)$ and $0.011(2)$ to express the deviation along the x, y, and z crystallographic direction, respectively. The modulations show clearly than the oxygen vacancies are not randomly distributed, but with a frequency of every three average unit cells, the two other ones being fully occupied (Fig. 4). Simultaneously, the Mn atoms present a small displacement along the a and c direction which implies a variation of the Mn–O distances. Therefore modulation waves could be associated in that class of materials with a variation of the covalence charge on the Mn site. Such types of modulation waves have already been observed for $LiMn_2O_4$ during delithiation.[40]

As presented in Fig. 3b, annealing the $LiMn_2O_4$ sample introduces major modifications on the crystal structure of the material. First, the inset of the Fig. 3b shows that splitting of the $(004)_c$ reflection is no longer observed, and therefore the final refinement was carried out using $Fd\overline{3}m$ symmetry. Notice that the asymmetry of the peak associated with a strong Lorentzian component in the profile shape indicates some degree of defects in the crystal structure. The final refinement converge smoothly to a satisfactory $R = 3.40\%$ for a G.o.F. = 2.1. The cell parameters, atomic positions and equivalent atomic displacement are listed in Table 3. Importantly, the oxygen position is fully occupied, and additional residues localized near $(0, 0.26, 0.73)$ could be eventually associated with some excess oxygen atoms (0.03 oxygen), which we observe by thermogravimetric analysis and will be described in the next section. This residual electron density is located on the generic Wyckoff position $(192i)$, which is within a reasonable Mn–O covalent bonding distance ($\sim$1.96 Å). This site is illustrated in Fig S4.†

Table 2 Atomic parameters, occupancies and equivalent displacement parameters (Å²) for $LiMn_2O_{3.96}$ synthesized in air

Atom	Wyckoff site	Occ.	x	y	z	U_{eq}
Li	8a	1	0.125	0.125	0.125	0.0061(10)
Mn	16d	1	0.5	0.5	0.5	0.0042(7)
O	32e	0.96(1)	0.7387(4)	0.7378(5)	0.7353(6)	0.0082(9)

Table 3 Atomic parameters, occupancies and equivalent displacement parameters ($\mathring{A}^2$) for air annealed $LiMn_2O_{4.03}$ (cell parameter: $a = 8.2304(5)$ $\mathring{A}$)

Atom	Wyckoff site	Occ.	x	y	z	U_{eq}
Li	8a	1	0.125	0.125	0.125	0.0134(11)
Mn	16d	1	0.5	0.5	0.5	0.0081(3)
O	32e	1	0.26324(6)	0.26324(6)	0.26324(6)	0.0140(3)

The hypothesis developed from our structural and elemental analyses is that although cation substitution and oxygen non-stoichiometry are prevalent in materials prepared *via* hydrothermal synthesis, annealing the samples eliminates (at least minimizes beyond all detection, *vide infra*) oxygen vacancies. The distinct advantage of this approach compared to solid-state preparative methods is that soft chemical routes give rise to nanoparticles that will show much greater rate capability. The remainder of the results section details the experimental data supporting this hypothesis. We will illustrate the impact of synthesis conditions, which dictate structure and composition, on the electrochemical performance of these materials as cathodes for lithium-ion batteries. Specific attention is given to the initial capacity, the capacity retention, and rate capability of the resulting cells.

4. Substantiating the presence of oxygen vacancies by TGA, DSC, and CV

Thermogravimetric analysis, differential scanning calorimetry, and cyclic voltammetry verify the qualitative presence of oxygen vacancies, as has been well discussed in the lithium manganospinel literature.[8,34,41,42] Fig. 5 shows that all hydrothermally synthesized spinel samples as well as their annealed analogues lose up to 1% mass upon heating to 200 °C by TGA, attributed to the loss of surface water from the nanocrystalline material. This assignment is corroborated by FTIR spectroscopy (Fig S5†); materials stored in the ambient room atmosphere show prominent ν(O–H) vibration and δ(H–O–H) bending modes at 3300 and 1630 cm^{-1} respectively.

First, we focus on the air- and N_2-synthesized samples. The TGA in Fig. 5 a–b shows a mass gain between 200–300 °C: 0.11% for the sample synthesized in air, 0.10% for the sample prepared under N_2. However, TGA of the corresponding annealed samples in Fig. 5 c–d shows no such gain in mass. This observation is understood by eqn (5) and (6) from the first section of the results: oxygen vacancies are already filled by annealing, therefore no additional mass increase can occur. Important to this interpretation, a control experiment in which the TGA of the compound synthesized in air was performed under a nitrogen purge shows no such mass increase (Fig S6†). Above ~330 °C, all samples show a mass decrease, as has been described in the chemistry of materials prepared at high temperature.[30,32] In our samples, this indicates that perhaps our hydrothermally synthesized compounds absorb excess oxygen at these low annealing temperatures. We will return to this point in the next section.

Next, DSC measurements further support a change in the oxygen stoichiometry of hydrothermally synthesized samples. At ~280 K, lithium manganospinel undergoes a phase transition

from the cubic structure ($Fd\bar{3}m$) to what was originally identified as a phase having tetragonal symmetry ($I4_1/amd$),[43] though later shown to be orthorhombic ($Fddd$) by synchrotron X-ray diffraction.[44] This first-order phase change is attributed to partial columnar charge ordering,[45] and can be observed in the DSC. Fig. 6 a–b shows that prior to annealing, the material synthesized in either ambient air or under a pure N_2 atmosphere shows the transition as an exotherm at 8.7 and 7.7 °C, respectively with an enthalpy change of 2.10 and 3.65 J g^{-1}, respectively. This phase transition no longer appears after annealing the samples since Z_{Mn} increases to 3.57 and 3.55 for air and N_2 samples, sufficient to suppress the symmetry-lowering distortion.[46]

Then, cyclic voltammetry points to the presence of oxygen vacancies within hydrothermally synthesized materials. Fig. 7 shows the voltammograms of spinel materials prepared by hydrothermal synthesis. Upon charging, all materials show two oxidation waves at 4.13 V and 4.26 V (*vs.* Li$^+$/Li) with corresponding reduction waves at 3.81 V and 4.02 V upon discharge. These correspond to the one-electron oxidation of Mn^{3+} to Mn^{4+} with lattice contraction/expansion at $^1/_2$ charge/discharge. The change in lattice parameter and resultant shift in chemical potential was described in the first report of lithium manganospinel.[5] Interestingly, the as-prepared hydrothermal samples synthesized under air and under N_2 display an additional wave at $E_{1/2}$ of ~3.25 V, previously shown to be attributed to oxygen vacancies formed in the structure as electrons are transferred to the electrolyte.[32,47] This results in a phase transition to a double hexagonal structure, as has been shown in previous HR-TEM studies.[48] Once annealed, the disappearance of this wave suggests that such a mechanism is no longer operable in these samples.

Finally, we consider together the data for lithium manganospinel synthesized under a pure O_2 atmosphere. TGA shows a small mass gain of 0.05% between 200–300 °C, and it disappears after annealing, just as was the case for the air and N_2 samples. In the DSC, no exotherm near 280 K is observed in either the synthesized or the annealed sample, despite Z_{Mn} being slightly less than +3.5 in the synthesized compound (3.47). Finally, the compound prepared under an O_2 atmosphere shows no discernable wave at $E_{1/2}$ of ~3.25 V in its cyclic voltammogram. Together, the DSC and CV results hint that the oxygen mole fraction of 3.96 in the synthesized sample is sufficient to prevent charge ordering. Furthermore, the lack of oxygen vacancies in the O_2 annealed sample indicates that this material will result in superior electrochemical performance.

5. Measuring the capacity and reversibility as a function of oxygen vacancies

In order to assess the promise of hydrothermally synthesized materials as practical electrodes, we performed galvanostatic cycling under three sets of conditions. First, we recorded three charge-discharge cycles at a rate of *C*/10. Here, the initial capacities were determined as well any changes in the voltage profile as the solid-electrolyte interface (SEI) layer is forming. As shown in Fig. 8, all spinel compounds show an initial discharge capacity between 115 and 120 mAh/g. For the air synthesized sample, the capacity fades to 106 mAh/g with the third cycle. The annealed compound still has a capacity of 117 mAh/g on the third cycle. Slow cycling gives the best measure of total available
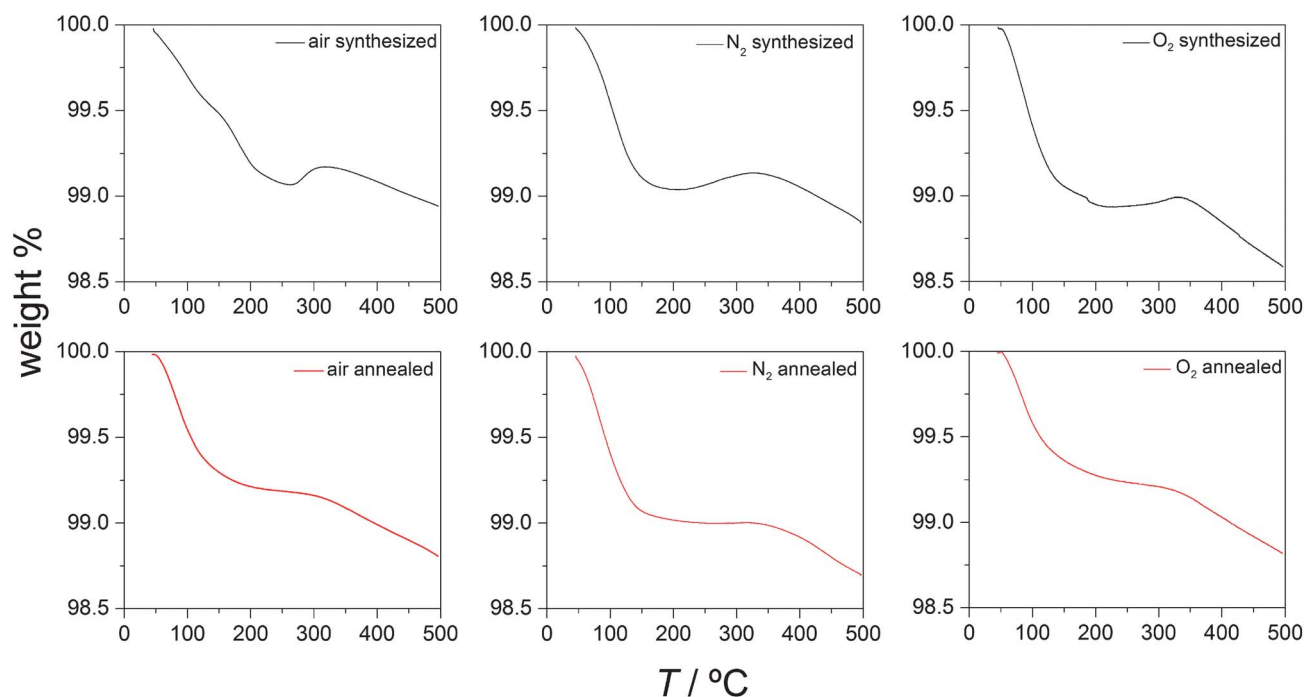
Fig. 5 TGA traces of lithium manganospinels synthesized by hydrothermal methods.

capacity as lithium in the core of the material has sufficient time to diffuse to the surface and allows us to determine the cycle-to-cycle Coulombic efficiency, q_{out}/q_{in}. For the third charge/discharge cycle, the measured Coulombic efficiency of hydrothermally synthesized materials ranges from 94.83% (air synthesized sample) to 98.60% (O_2 synthesized sample). Of course, three slow cycles do not translate directly into the practical utility of an electrode, so we then constructed a second set of cells that were charged and discharged at the faster rate $C/3$, and the first one hundred cycles were recorded. The data are shown in Fig. 9 and summarized in Table 1, with the individual charge-discharge curves for every 20th cycle available in Fig S7.† Upon discharge from 4.45 V, a flat plateau is observed at 4.1 V through $1/2$ discharge, followed by a gently sloping voltage profile centered about 3.9 V to complete discharge. This suggests a two-phase region upon initial discharge, followed by an alloyed region. The fade in capacity is least for the samples prepared

under O_2, 10.0 and 6.1% for the as synthesized and annealed compounds respectively.

Here, we must address why we anneal at 500 °C given our TGA results where maximum oxygen uptake occurs between 310 and 330 °C. Experimentally, we performed two experiments summarized here with data presented in Fig S8.† First, we annealed the air synthesized compound at 310 °C and observe that over the first ten cycles, the capacity is stable, but significantly lower, only 81 mAh/g. We annealed a second sample at the weight-loss threshold, 270 °C and observe a similar result—the capacity is nearly constant over the first ten cycles, but is only 73 mAh/g. X-ray diffraction performed on these compounds shows that the lattice parameters of these compounds are 8.219 and 8.216 Å respectively. In addition, potentiometric titration shows that Z_{Mn} significantly greater than 3.5 for these compounds (3.68 and 3.66 respectively), which explains the low gravimetric capacities. This is supported further by the lack of
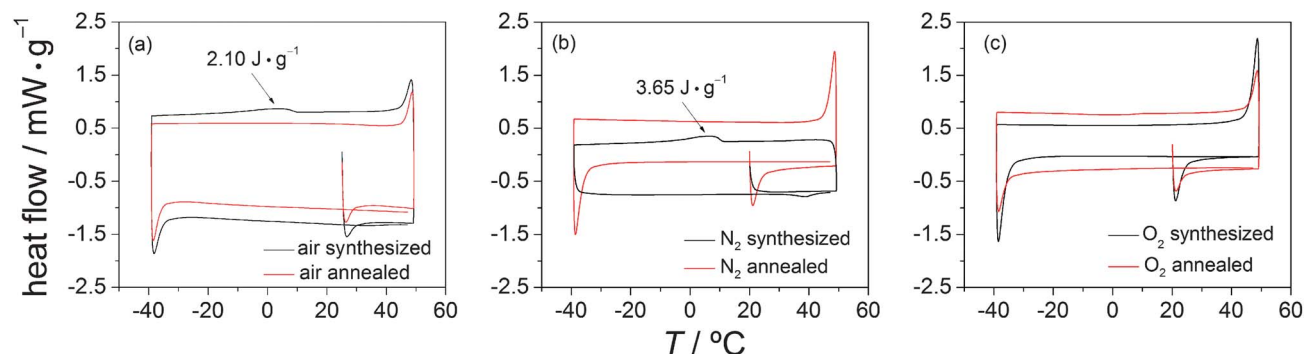
Fig. 6 DSC traces for lithium manganospinels synthesized in a) air; b) N_2; c) O_2. Black and red curves represent the synthesized and annealed samples, respectively.

This journal is © The Royal Society of Chemistry 2012

J. Mater. Chem., 2012, **22**, 1578–1591 | 1585
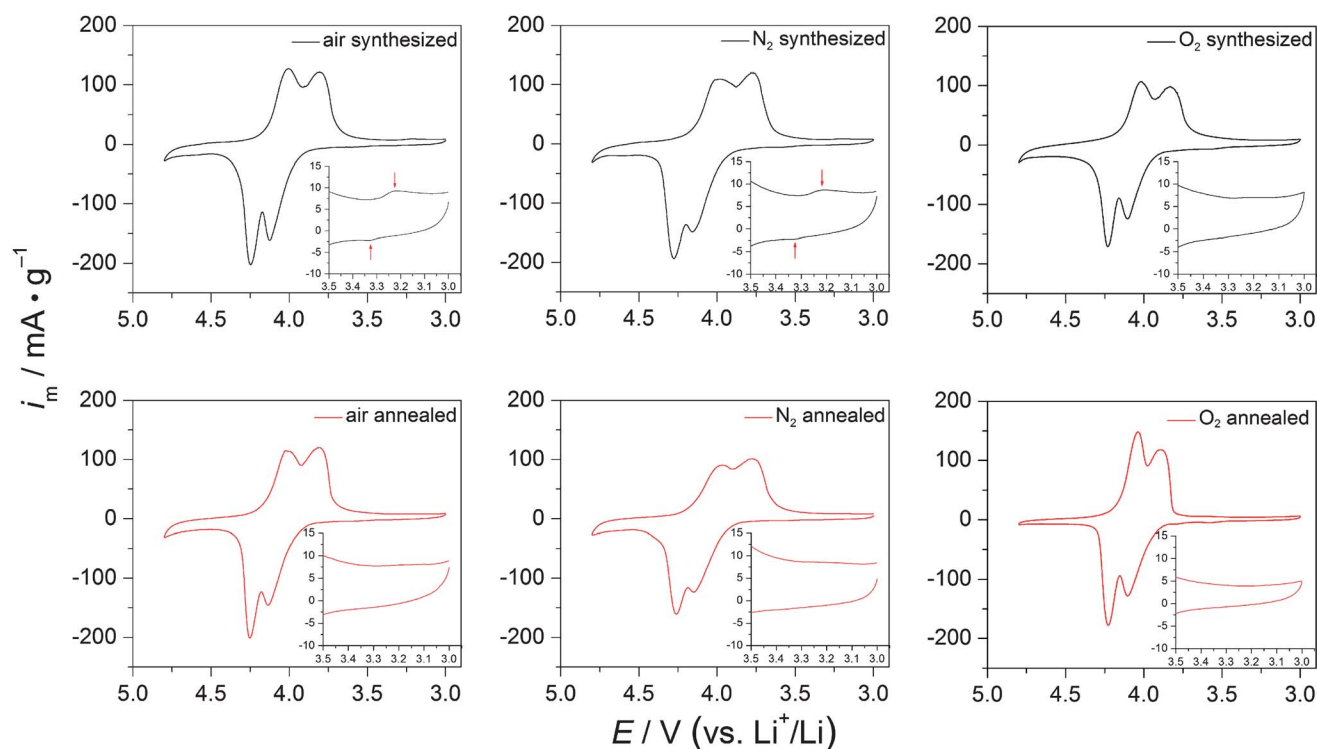
Fig. 7 Cyclic voltammograms of lithium manganospinels. Black traces in the top panel are for the synthesized samples. Red traces in the bottom panels are for the corresponding annealed samples. The inset blows up the region between 3.5 and 3.0 V where an additional wave can be observed for the air and N_2 synthesized samples (noted by the red arrows).
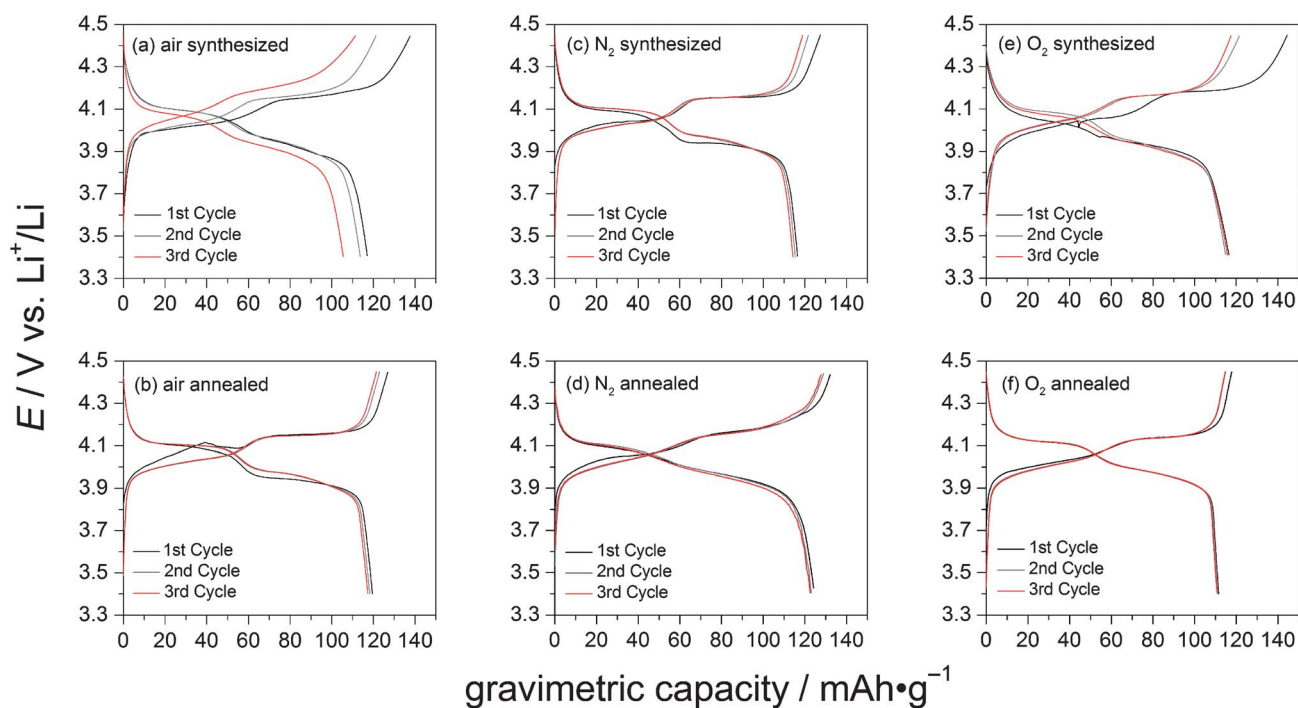
Fig. 8 First three charge-discharge curves recorded at rate $C/10$ for lithium manganospinels. Black, gray, and red curves represents cycles one, two, and three respectively.

a constant voltage plateau in the galvanostatic cycling, shown for the 10th cycle of these two samples in Fig S8.† This indicates that upon discharge from 4.45 V, Z_{Mn} is sufficiently high such that Li insertion occurs in a single phase, not the typical two-phase mixture.[49] By annealing at 500 °C, both the composition changes (from oxygen deficient to a slight excess of oxygen), and the
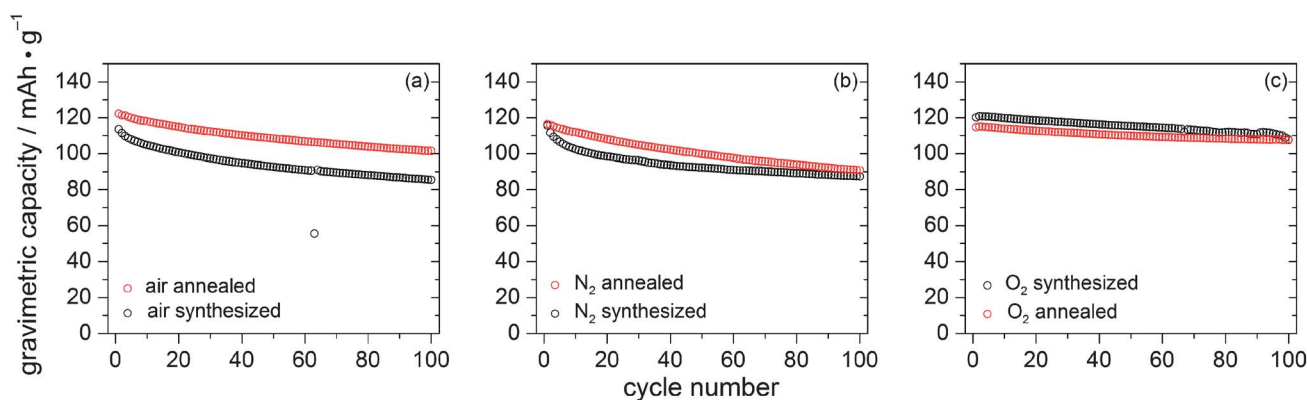
Fig. 9 Galvanostatic cycling at current $C/3$ for lithium manganospinel synthesized hydrothermally in a) air; b) nitrogen; and c) oxygen. Black and red circles represent the synthesized and annealed samples, respectively. The anomalous data point at cycle 63 for the air synthesized sample arises because the computer had to be restarted during that measurement.

structure changes (no orthorhombic superspace group is observed by PND) to give lithium manganospinel with high capacity.

Returning to the best sample with respect to capacity retention, the O_2 sample annealed at 500 °C, cycling was performed at varying rate to demonstrate its utility in high power applications. Fig. 10 illustrates that at a charge/discharge rate of $3C$, the O_2 annealed sample demonstrates an initial discharge capacity of 112 mAh/g with 95.6% retention (108 mAh/g) after 100 cycles. This is nearly identical to the observed capacity and retention of at the slower rate of $C/3$. When the material is cycled at the even faster rate of $5C$, the capacity is slightly lower, 99 mAh/g. Again, however, 95.6% of this capacity is retained (95 mAh/g) after 100 cycles.

Moreover, the O_2 annealed sample shows excellent cycling behavior at elevated temperature. This is important because the detrimental surface disproportionation of Mn^{3+} becomes more facile as temperature increases, and the majority of capacity fade is observed within the first 15 cycles.[50] In the case of our lithium manganospinel nanoparticles, cycling the material with constant current of $5C$ at 55 °C shows an initial capacity of 99 mAh/g that fades to only 88 mAh/g after 100 cycles (88.9% capacity retention).

Together, these data suggest that lithium-ion diffusion is rapid in the sample. To verify that lithium-ion diffusion is indeed rapid, we performed electrochemical impedance spectroscopy. Fig. 11 shows the voltage-dependence of the lithium-ion diffusion constant with Nyquist plot and fit of the data collected at 4.15 V to the equivalent circuit illustrated.[51] The Nyquist plot shows three discernable semicircles corresponding physically to transport through the SEI layer, electronic reorganization associated with localized $Mn^{3+/4+}$ charge hopping, and charge transfer, as has been recently described.[52] Then, the low frequency Warburg impedance (Z_W) is related to the lithium-ion diffusion constant (D_{Li}) by the equation[53]

$$Z_W = \frac{V_m\left(\frac{dE}{dx}\right)}{FA(2D_{Li})^{1/2}} \quad (7)$$

where V_m is the molar volume of lithium manganospinel (140 cm³ mol⁻¹), dE/dx, the slope of coulometric titration, is determined

from cyclic voltammetry at 0.1 mV s⁻¹, F is Faraday's constant and A is the electrode surface 500 cm². The Nyquist plots for the compound cycled to other potentials are included as Fig S9.† For the O_2 annealed sample, D_{Li} is on the order of 10^{-7} to 10^{-9} cm² s⁻¹, rapid indeed, but on par with has been determined by EIS for
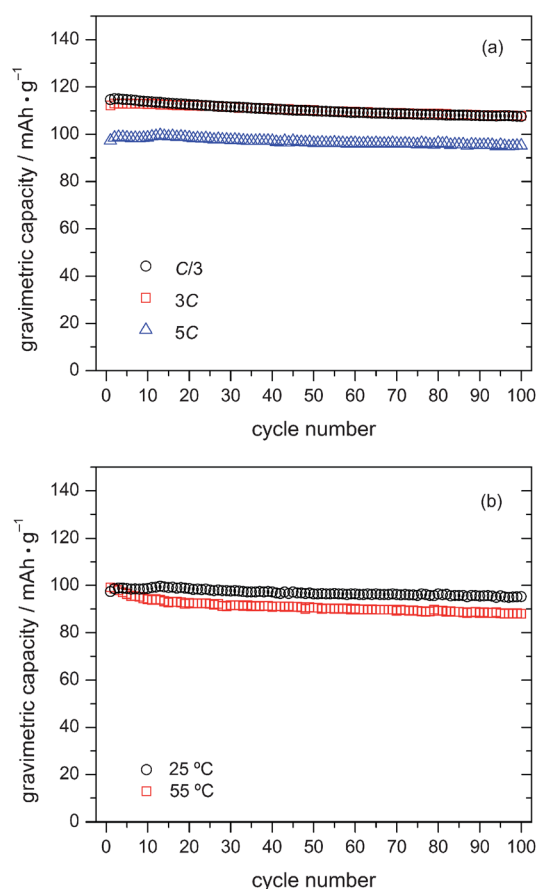
Fig. 10 a) Rate capability of lithium manganospinel synthesized under O_2 followed by annealing in air. Black circles, red squares, and blue triangles represent cycling at currents corresponding to the rates $C/3$, $3C$, and $5C$ respectively; b) Temperature-dependence of galvanostatic cycling at $5C$.
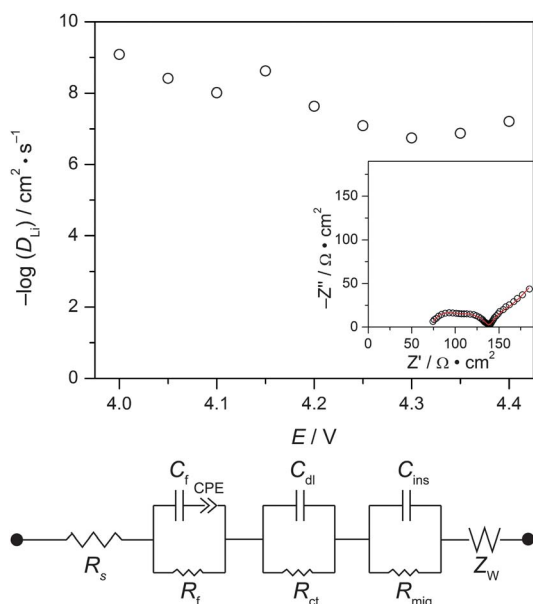
Fig. 11 Lithium-ion diffusion constant as a function of potential determined by EIS. Inset. Nyquist plot for the 4.15 V data. The data (black circles) are fit (red line) to the equivalent circuit is illustrated below the main plot.

lithium manganospinel prepared by sol–gel methods.[54] This rapid Li-ion diffusion supports the conclusion that our nanoscale material prepared under O_2 followed by annealing shows a rate capability and gravimetric energy density that is at least on par with, if not exceeds even the best material prepared by solid-state synthesis.

Discussion

Oxygen vacancies in the Li–Mn–O spinel system have been long recognized in the solid-state literature,[55] predating the concept of energy storage by electrochemical Li^+ insertion and extraction. In this original study, it is shown that the lithiated cubic spinel phase reacts with hausmannite, Mn_3O_4 according to the reaction:

$$LiMn_2O_4 + Mn_3O_4 \rightarrow LiMn_2O_{3.5} + {}^1/_2 O_2 \quad (8)$$

Hausmannite also belongs to the spinel group ($Mn^{2+}Mn^{3+}{}_2O_4$), and is a common impurity phase encountered during lithium manganospinel synthesis. In addition to reaction with hausmannite, oxygen vacancies are introduced into lithium manganospinel synthesized under reducing conditions such as ammonia reduction[31] or rapid quenching of solid-state reactions performed in air[8,34] Beyond the preparation of oxygen non-stoichiometric materials, there are several proposed thermodynamic models for vacancy formation on the surface.[56–58] Notably, after our annealing treatment, we do not observe any secondary phases by PND such as Mn_3O_4 or Li_2MnO_3 that frequently result from high-temperature processing.[59]

Crystal distortions that arise from the presence of Mn^{3+} in the spinel structure were also recognized long before the electrochemistry was studied.[60] As mentioned in the introduction, oxygen vacancies result in materials with poor electrochemical performance, and an empirical set of guidelines for optimizing

the performance of lithium manganospinel has been published.[61] Our work is aimed at the first principle: to establish stoichiometry resulting from synthesis and any treatments applied prior to cell assembly. The hydrothermal reaction employed in our lab provides the most oxidized product when carried out under an oxygen atmosphere. The role of reaction atmosphere is not unique to hydrothermal synthesis, however. In preparing stoichiometric spinel from lithium hydroxide and either chemically prepared manganese dioxide[10] or γ-MnOOH[11] in a muffle furnace, the reaction proceeds most cleanly under a reducing nitrogen atmosphere to prevent the decomposition reaction to form Li_2MnO_3. In this reaction, the culprit is oxidation of Mn^{3+} in $LiMn_2O_4$ by atmospheric O_2.

In stark contrast, hydrothermal conditions do not yield stoichiometric lithium manganospinel, rather material with oxygen vacancies. The initial precipitate from the reaction of potassium permanganate with acetone has the layered δ-MnO_2 birnessite structure. ICP-AES (to determine Li, K, and Mn mole ratios) and potentiometric titration (Z_{Mn} of 3.69) of this isolable intermediate gives the formula $Li_{0.23}K_{0.16}MnO_{2.04} \cdot 1.25 H_2O$.

This initial precipitate is at least stoichiometric in oxygen, perhaps with a slight excess of oxygen. Therefore, we surmise that oxygen vacancies could be easily introduced into the spinel structure to support electroneutrality, perhaps as potassium is expelled from the structure and replaced by lithium; notably, there is no potassium present in our spinel product. The fact that oxygen vacancies persist in our material regardless of the atmosphere under which the reaction proceeds suggests that our hydrothermal reaction conditions are reducing from the standpoint of the solid oxide product. To demonstrate further the reducing environment of our reaction, Fig. 12 shows the lattice parameter and the average manganese valence of the solid spinel product obtained *ex situ* at varying reaction times. Indeed, we observe an increase in the lattice parameter and decrease in the average manganese valence as the reaction proceeds, *even in a pure O_2 atmosphere*. This hints at the need to anneal our materials in an oxidizing environment after hydrothermal synthesis. Empirically, maximum weight uptake occurs at ~310 °C, but we find that Z_{Mn} is large, 3.66, leading to low overall capacity. Notable is that the particle size and cation composition are conserved in our annealing procedure, which is different from what is observed in ref. 21, where annealing at 800 °C results in consumption of nanoparticles to form micron-sized particles.

The unique aspect of our synthesis work is discovering the structural complexity of compounds synthesized by hydrothermal methods. The results from our neutron diffraction data show that Mn^{3+} and/or oxygen vacancies lead to symmetry lowering, which has large implications on the electrochemistry of the material, particularly the capacity retention. The *Fddd* orthorhombic structure that we observe has been previously reported for both stoichiometric $LiMn_2O_4$[62] as well as for non-stoichiometric $LiMn_2O_{4-\delta}$ prepared by calcination at temperatures above 800 °C.[63] We note that this superstructure is not discernible using standard laboratory Cu-Kα radiation at room temperature. However, after annealing the sample, this superstructure is no longer observable in the room-temperature powder neutron diffraction; the only observable reflections are the Bragg peaks from the cubic $Fd\bar{3}m$ space group, similar to what has been observed for other stoichiometric spinels synthesized by

1588 | J. Mater. Chem., 2012, **22**, 1578–1591

This journal is © The Royal Society of Chemistry 2012
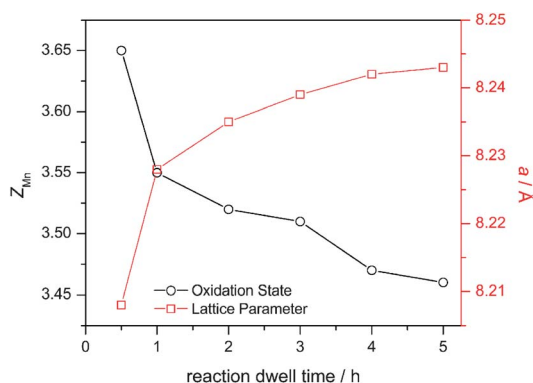
Fig. 12 Average manganese oxidation state (black) and lattice parameter (red) or lithium manganospinel synthesized by hydrothermal methods in air as a function of dwell time.

ceramic routes.[64] These cubic nanoparticles cycle with greater capacity retention without the need for particle coatings.

Then, from the perspective of power, our synthesis of small particles is advantageous because they are less susceptible to fracture. Volume changes in nanoparticles are more readily accommodated, giving rise to the excellent rate capability and capacity retention in the compound. Although there are several examples of using hydrothermal methods to prepare lithium manganospinel nanoparticles, Table 4 shows that the capacity retention from these preparations is often quite poor. Our work here suggests that preparing nanoparticles is not an inherent problem with lithium manganospinel. Rather, it is the composition (and perhaps the concomitant structural implications) that results in poor performance—namely the presence of oxygen vacancies which increases the Jahn–Teller distortive Mn^{3+} concentration. Although this fact is recognized in several of the references in Table 4, we have addressed the matter experimentally. The closest comparison in the table is ref. 23, however there is no specific mention of nonstoichiometric composition therein.

Table 4 Electrochemical properties of spinels synthesized by hydrothermal conditions

Nominal composition	Capacity at 4 V plateau (mAh/g)	Capacity retention/# cycles	Reference
$Li_{0.96}Mn_{2.04}O_{4.05}$	107[a]	75%/10	15
$Li_{1.08}Mn_{1.92}O_{3.97}$	92[a]	91%/10	15
$Li_{1.23}Mn_{1.77}O_{3.87}$	66[a]	95%/10	15
$Li_{0.90}Mn_2O_{3.95}$	~92 unstated	data not presented	19
$Li_{1.25}Mn_{1.75}O_{3.98}$	110 at C/2	82%/10	18
$LiMn_2O_4$	130 at C/10	>95%/60	21
$Li_{0.92}Mn_2O_4$	107 at C/3	84%/50	22
$LiMn_2O_4$	91 at 8C	96%/100	23
$LiMn_2O_4$	113 at C/5	93%/20	24
$LiMn_2O_4$ nanorods	100 at 1 C	85%/100	25
$LiMn_2O_4$	95 at 1.6 C	79%/30	26
$LiMn_2O_4$	87 at C/10	85%/25	27
$LiMn_2O_4$	98 at C/2	88%/50	28
$Li_{1.01}Mn_{1.99}O_{4.07}$	115 at C/3	94%/100	this work
	113 at 3C	96%/100	
	99 at 5C	94%/100	

[a] 200 μA cm^{-2} current using a 10 mm diameter electrode.

There, the increase in lattice parameter as a function of time suggests that oxygen vacancies may be present, and we note that only after three days is highly electroactive spinel isolated in the absence of an organic reducing agent. Our materials, attainable in less than a day, show exceptional stability even at elevated temperatures and relatively rapid rates.

In order to show that nanoparticles synthesized in O_2 and annealed in air do indeed yield stable electrodes, we performed an experiment in which a cathode composed of 5.5 mg of lithium manganospinel was immersed in 10 mL electrolyte solution (1 M $LiPF_6$ in 2 : 1 EC:DEC). The manganese concentration of manganese in the electrolyte was measured after soaking the electrode for 24 h. This experiment was performed twice—once on a cell at open circuit, and again for a cell held at 4.45 V vs. Li^+/Li (our maximum operating voltage, where the mole fraction of Mn^{4+} is highest). In both of these experiments, the amount of manganese lost to the electrolyte solution is 0.10%, significantly less than a comparable test performed on pure uncoated spherical micron-sized particles.[65]

From the perspective of the Li–Mn–O phase diagram, we cannot yet say where these compositions fall, although current efforts in are group are focused on elucidating the phase relationships. The phase diagram in air at elevated temperature has been well established[66–68] and a Pourbaix-like pH-stoichiometry diagram for lithium manganospinels in acid has been recently determined,[69] but relatively little is known regarding the phase equilibria present under basic hydrothermal conditions. Here, we can only conclude that our results of having both cation mixing and oxygen vacancies are consistent with the phase relationships of lithium manganospinels prepared from ceramic/calcination methods above 900 °C, where $Li_{1+x}Mn_{2-x}O_{4-\delta}$ is proposed to be thermodynamically stable. Electrochemically, we observe superior capacity retention in compounds stoichiometric in oxygen, more akin to what is observed in the cation-deficient, Li-rich spinels.[70]

Here, we must discuss the potential technological advances initiated by the nanomaterials materials we have prepared. It has been suggested in the literature that the loss of cyclability in lithium manganospinel at both room temperature and elevated temperature does not originate from structural transformations per se, rather with the composition: the greater the mole fraction of Mn^{3+} in the compound, the greater the degradation.[71] We find that hydrothermal synthesis gives material that is deficient in oxygen and has an orthorhombic superstructure. These two features are not mutually exclusive, so it remains undetermined which factor is more important. That is, we cannot answer here the question: is electrochemical performance is enhanced simply by filling in vacancies or is it due to the loss of orthorhombic superstructure after annealing? At best, our results show that the Mn^{3+} concentration in the hydrothermally synthesized orthorhombic product is larger and there is oxygen nonstoichiometry. After annealing, electrons are transferred from Mn^{3+} to surface oxygen, giving cubic compounds with Z_{Mn} larger than 3.5. At this point, the new chemistry stimulated in this well-studied material is that annealing nanoparticles synthesized hydrothermally using organic reducing agents such as acetone affords high rate capability. The novel aspect here is that it is simply structure and composition that results in high performance electrodes, not nano-architecture.

This journal is © The Royal Society of Chemistry 2012

J. Mater. Chem., 2012, **22**, 1578–1591 | 1589

Finally, we have largely focused on power, but must also comment on the energy density of nanomaterials. In order to achieve a large *volumetric* energy density, the tap density is critical.[72] We have crudely measured the tap density of our nanoparticles (using a balance, a graduated cylinder, and a No. 2 pencil), and find that it is 1.2 g cm^{-3}, on par with lithium manganospinel prepared by other low temperature routes,[73] despite a significantly larger surface area according to our N_2 isotherms. As observed in the SEM images, our nanoparticles agglomerate readily and EIS shows that Li$^+$ diffusion is rapid. Further exploration is needed to optimize the carbon-coating levels to determine the packing density required for a practical battery. However, our results here are promising: the same gravimetric capacity attainable at the rate $C/3$ and $3C$ hints that a battery composed of our lithium manganospinel can be charged completely in 20 min. As a benchmark for the rate capability of our materials, the measured reversible capacity of 99 mAh/g at $5C$ (0.67 mol Li extracted) is greater than the literature-reported capacity at $2.5C$ for micron-sized particles, $\sim$81 mAh/g (0.55 mol of Li extracted).[74] At present, we are exploring the generality of using organic oxidation reactions under hydrothermal conditions followed by annealing to prepare other manganese-containing oxide nanomaterials for high power electrical energy storage.

Conclusions

Lithium manganospinel nanoparticles prepared by hydrothermal methods has been shown to contain oxygen vacancies by the combination of TGA, DSC, CV, and PND characterization regardless of the environment under which the reaction is performed. However, these vacancies can be eliminated beyond the detection limits of all analytical methods by annealing the synthesized compounds at 500 °C in air for 4 h. In addition, the hydrothermally synthesized sample shows an orthorhombic *Fddd* (α00) supergroup that disappears upon annealing. As a result, the material prepared under the most oxidizing conditions (synthesized under an autogenous pressure of O$_2$, followed by annealing) shows the highest reversibility under various cycling conditions—$C/3$, $3C$, $5C$, and $5C$ at 55 °C. This behavior is observed without having to coat our particles (beyond the typical use of carbon to enhance electrical conductivity) or insert compositional complexity in the form of nickel and/or cobalt on the octahedral lattice sites. Li-ion diffusion, measured by EIS, is found to be rapid, which explains the high rate capability. Current efforts are aimed at elucidating phase relationships within materials prepared by hydrothermal methods in order to examine the influence of cation stoichiometry and composition on the rate capability of nanoparticles, building on the larger body of lithium manganospinel literature. In addition, we are modifying our low-temperature hydrothermal preparation methods to synthesize spinel particles in a range of sizes from the nanometre to tens of micron-scale to compare oxygen vacancy content, capacity, and rate capability.

Acknowledgements

References

1 M. Yoshio and H. A. H. Noguchi, Review of Positive Electrode Materials for Lithium-Ion Batteries, in *Lithium-Ion Batteries: Science and Technology*, ed. Yoshi, M., Brodd, R. J., Kozawa, A., Springer, New York, 2010, pp 17–30.
2 M. M. Thackeray, A. de Kock, H. Rossouwm, D. Liles, R. Bittihn and D. Hoge, *J. Electrochem. Soc.*, 1992, **139**, 363.
3 D. G. Wickham and W. J. Croft, *J. Phys. Chem. Solids*, 1958, **7**, 351.
4 M. M. Thackeray, W. I. F. David, P. G. Bruce and J. B. Goodenough, *Mater. Res. Bull.*, 1983, **18**, 461.
5 M. M. Thackeray, P. J. Johnson, L. A. de Picciotto, P. G. Bruce and J. B. Goodenough, *Mater. Res. Bull.*, 1984, **19**, 179.
6 R. J. Gummow, A. de Kock and M. M. Thackeray, *Solid State Ionics*, 1994, **69**, 59.
7 A. Manthiram, A. V. Murugan, A. Sarkar and T. Muraliganth, *Energy Environ. Sci.*, 2008, **1**, 621.
8 J. M. Tarascon, W. R. McKinnon, F. Coowar, T. N. Bowmer, G. Amatucci and D. Guyomard, *J. Electrochem. Soc.*, 1994, **141**, 1421.
9 A. Momchilov, V. Manev and A. Nassalevska, *J. Power Sources*, 1993, **41**, 305.
10 Y. Xia, H. Takeshige, H. Noguchi and M. Yoshio, *J. Power Sources*, 1995, **56**, 61.
11 Y. Xia and M. Yoshio, *J. Power Sources*, 1995, **57**, 125.
12 Y. Xia, Y. Zhou and M. Yoshio, *J. Electrochem. Soc.*, 1997, **144**, 2593.
13 A. S. Aricò, P. Bruce, B. Scrosati, J.-M. Tarascon and W. van Schalkwijk, *Nat. Mater.*, 2005, **4**, 366.
14 Q. Feng, H. Kanoh, Y. Miyai and K. Ooi, *Chem. Mater.*, 1995, **7**, 1226.
15 T. Kanasaku, K. Amezawa and N. Yamamoto, *Solid State Ionics*, 2000, **133**, 51.
16 Q. Feng, Y. Higashimoto, K. Kajiyoshi and K. Yanagisawa, *J. Mater. Sci. Lett.*, 2001, **20**, 269.
17 Y. C. Zhang, H. Wang, H. Y. Xu, B. Wang, H. Yan, A. Ahniyaz and M. Yoshimura, *Solid State Ionics*, 2003, **158**, 113.
18 Z. Liu, W.-L. Wang, X. Liu, M. Wu, Z. Zeng and D. Li, *Inorg. Chem. Commun.*, 2004, **7**, 308.
19 Y. Lu, M. Wei, Z. Wang, D. G. Evans and X. Duan, *Electrochim. Acta*, 2004, **49**, 2361.
20 Z. Liu, W.-L. Wang, X. Liu, M. Wu, D. Li and Z. Zeng, *J. Solid State Chem.*, 2004, **177**, 1585.
21 K. Kanamura, K. Dokko and T. Kaizawa, *J. Electrochem. Soc.*, 2005, **152**, A391.
22 Y.-Y. Liang, S.-J. Bao, B.-L. He, W.-J. Zhou and H.-L. Li, *J. Electrochem. Soc.*, 2005, **152**, A2030.
23 C. H. Jiang, S. X. Dou, H. K. Liu, M. Ichihara and H. S. Zhou, *J. Power Sources*, 2007, **172**, 410.
24 X. Li, R. Xiang, T. Su and Y. Qian, *Mater. Lett.*, 2007, **61**, 3597.
25 D. K. Kim, P. Maualidharan, H.-W. Lee, R. Ruffo, Y. Yang, C. K. Chan, H. Peng, R. A. Huggins and Y. Cui, *Nano Lett.*, 2008, **8**, 3948.
26 H. Fang, L. Li, Y. Yang, G. Yan and L. Guangshe, *J. Power Sources*, 2008, **184**, 494.
27 P. Ragupathy, H. N. Vasan and N. Munichandraiah, *Mater. Chem. Phys.*, 2010, **124**, 870.
28 J.-W. Lee, J.-I. Kim and S. H. Min, *J. Power Sources*, 2011, **196**, 1488.
29 M. H. Rossouw, A. de Kock, L. A. de Picciotto and M. M. Thackeray, *Mater. Res. Bull.*, 1990, **25**, 173.
30 D. Guyomard and J. M. Tarascon, *Solid State Ionics*, 1994, **69**, 222.
31 M. N. Richard, E. W. Fuller and J. R. Dahn, *Solid State Ionics*, 1994, **73**, 81.
32 Y. Gao and J. R. Dahn, *J. Electrochem. Soc.*, 1996, **143**, 100.
33 Y. Chida, H. Wada and K. Shizuka, *J. Power Sources*, 1999, **81–82**, 454.

34 A. Yamada, K. Miura, K. Hinokuma and M. Tanaka, *J. Electrochem. Soc.*, 1995, **142**, 2149.
35 S. Ma, H. Noguchi and M. Yoshio, *J. Power Sources*, 2004, **126**, 144.
36 B. J. Liddle, S. M. Collins and B. M. Bartlett, *Energy Environ. Sci.*, 2010, **3**, 1339.
37 T. Marks, S. Trussler, A. J. Smith, D. Xiong and J. R. Dahn, *J. Electrochem. Soc.*, 2011, **158**, A51.
38 T. Janssen, *Crystallographic Groups*, North Holland, Amsterdam, 1973.
39 S. Van Smaalen, *Incommensurate Crystallography*, Oxford University Press, Inc., New York, 2007.
40 H. Björk, T. Gustafsson, J. O. Thomas, S. Lidin and V. Petřiček, *J. Mater. Chem.*, 2003, **13**, 585.
41 X. Q. Yang, X. Sun, M. Balasubramanian, J. McBreen, Y. Xia, T. Sakai and M. Yoshio, *Electrochem. Solid-State Lett.*, 2001, **4**, A117.
42 J. M. Amarilla and R. M. Rojas, *J. Therm. Anal. Calorim.*, 2003, **73**, 191.
43 A. Yamada and M. Tanaka, *Mater. Res. Bull.*, 1995, **30**, 715.
44 K. Oikawa, T. Kamiyama, F. Izumi, B. C. Chakoumakos, H. Ikuta, M. Wakihara, J. Li and Y. Matsui, *Solid State Ionics*, 1998, **109**, 35.
45 J. Rodríguez-Carvajal, G. Rousse, C. Masquelier and M. Herview, *Phys. Rev. Lett.*, 1998, **81**, 4660.
46 C. Masquelier, M. Tabuchi, K. Ado, R. Kanno, Y. Kobayashi, Y. Maki, O. Nakamura and J. B. Goodenough, *J. Solid State Chem.*, 1996, **123**, 255.
47 Y. Gao and J. R. Dahn, *Solid State Ionics*, 1996, **84**, 33.
48 L. Dupont, M. Hervieu, G. Rousse, C. Masquelier, M. R. Palacin, Y. Chabre and J. M. Tarascon, *J. Solid State Chem.*, 2000, **155**, 394.
49 T. Ohzuku, M. Kitagawa and T. Hirai, *J. Electrochem. Soc.*, 1990, **137**, 769.
50 B. Deng, H. Nakamura and M. Yoshio, *J. Power Sources*, 2008, **180**, 864.
51 D. Lu, W. Li, X. Zuo, Z. Yan and Q. Huang, *J. Phys. Chem. C*, 2007, **111**, 12067.
52 Q.-C. Zhuang, T. Wei, L.-L. Du, Y.-L. Cui, L. Fang and S.-G. Sun, *J. Phys. Chem. C*, 2010, **114**, 8614.
53 C. Ho, I. D. Raistrick and R. A. Higgins, *J. Electrochem. Soc.*, 1980, **127**, 343.
54 S. Bach, J. Farcy and J. P. Pereira-Ramos, *Solid State Ionics*, 1998, **110**, 193.
55 A. Bergstein and P. Kleinert, *J. Phys. Chem. Solids*, 1965, **26**, 1181.
56 J. Sugiyama, T. Atsumi, T. Hioki, S. Noda and N. Kamegashira, *J. Alloys Compd.*, 1996, **235**, 163.
57 J. Sugiyama, T. Atsumi, T. Hioki, S. Noda and N. Kamegashira, *J. Power Sources*, 1997, **68**, 641.
58 M. Wang and A. Navrotsky, *J. Solid State Chem.*, 2005, **178**, 1182.
59 M. M. Thackeray, M. F. Mansuetto, D. W. Dees and D. R. Vissers, *Mater. Res. Bull.*, 1996, **31**, 133.
60 D. B. Rogers, R. W. Germann and R. J. Arnott, *J. Appl. Phys.*, 1965, **36**, 2338.
61 G. Amatucci and J.-M. Tarascon, *J. Electrochem. Soc.*, 2002, **149**, K31.
62 G. Rousse, C. Masquelier, J. Rodríguez-Carvajal and M. Herview, *Electrochem. Solid-State Lett.*, 1999, **2**, 6.
63 R. Kanno, M. Yonemura, T. Kohigashi, Y. Kawamoto, M. Tabuchi and T. Kamiyama, *J. Power Sources*, 2001, **97–98**, 423.
64 R. Kanno, A. Kondo, M. Yonemura, R. Gover, Y. Kawamoto, M. Tabuchi, T. Kamiyama, F. Izumi, C. Masquelier and G. Rousse, *J. Power Sources*, 1999, **81–82**, 542.
65 X. He, J. Li, Y. Cai, Y. Wang, J. Ying, C. Jiang and C. Wan, *J. Power Sources*, 2005, **150**, 216.
66 Y. Xia and M. Yoshio, *J. Electrochem. Soc.*, 1997, **144**, 4186.
67 J. M. Paulsen and J. R. Dahn, *Chem. Mater.*, 1999, **11**, 3065.
68 M. Yonemura, A. Yamada, H. Kobayashi, M. Tabuchi, T. Kamiyama, Y. Kawamoto and R. Kanno, *J. Mater. Chem.*, 2004, **14**, 1948.
69 R. Benedek, M. M. Thackeray and A. van de Walle, *J. Mater. Chem.*, 2010, **20**, 369.
70 B. Deng, H. Nakamura and M. Yoshio, *Electrochem. Solid-State Lett.*, 2005, **8**, A171.
71 G. G. Amatucci, C. N. Schmutz, A. Blyr, C. Sigala, A. S. Gozdz, D. Larcher and J. M. Tarascon, *J. Power Sources*, 1997, **69**, 11.
72 H. Suzuki and Y. Nakayama, *Prog. Batt. Solar Cells*, 1984, **5**, 151.
73 X. M. He, J. J. Li, Y. Cai, Y. Wang, J. Ying, C. Jing and C. Wan, *J. Solid State Electrochem.*, 2005, **9**, 438.
74 Z. Jiang and K. M. Abraham, *J. Electrochem. Soc.*, 1996, **143**, 1591.